Journal of Immunology and Regenerative Medicine 12 (2021) 100041

Contents lists available at ScienceDirect

Journal of Immunology and Regenerative Medicine

journal homepage: www.elsevier.com/locate/regen

Extracellular matrix scaffolds derived from different musculoskeletal tissues drive distinct macrophage phenotypes and direct tissue-specific cellular differentiation

Olwyn R. Mahon [a,c,e,1,*], David C. Browe [c,d,e,1], Pedro J. Diaz-Payno [c,d], Pierluca Pitacco [c,d], Kyle T. Cunningham [a], Kingston H.G. Mills [a], Aisling Dunne [a,b,e,1], Daniel J. Kelly [c,d,e,1]

[a] School of Biochemistry and Immunology, Trinity College Dublin, Dublin, Ireland
[b] School of Medicine, Trinity College Dublin, Dublin, Ireland
[c] Trinity Centre for Biomedical Engineering, Trinity Biomedical Sciences Institute, Trinity College Dublin, Dublin, Ireland
[d] Department of Mechanical, Manufacturing and Biomedical Engineering, School of Engineering, Trinity College Dublin, Dublin, Ireland
[e] Advanced Materials and Bioengineering Research (AMBER) Centre, Trinity College Dublin, Ireland

ARTICLE INFO

Keywords:
Musculoskeletal extracellular matrix
Biologic scaffold
Macrophage polarization
Immune cells
Hybrid phenotype
Vascularisation

ABSTRACT

The host immune response, specifically macrophage function, is a critical determinant of biomaterial success or failure post-implantation. Extracellular matrix (ECM) derived scaffolds have been shown to promote a pro-regenerative macrophage phenotype and a more constructive remodelling outcome. Here we demonstrate that macrophages adopt distinct phenotypes when exposed to articular cartilage (AC), ligament (LIG) and growth plate (GP) derived ECM scaffolds. Macrophages were generally unresponsive to LIG-derived ECM, adopted an M2-like phenotype when exposed to AC-derived ECM, and a hybrid M1-M2 phenotype when exposed to GP-ECM. Furthermore, macrophages expressed higher levels of pro-chondrogenic factors, such as FGF2, when exposed to AC-ECM, and higher levels of angiogenic and pro-osteogenic factors, such as VEGF, IL-6 and TNF, when exposed to GP-ECM. In addition, we observed that they can differentially direct the differentiation of skeletal stem cells, whereby AC-ECM promotes the chondrogenic differentiation and GP-ECM the osteogenic differentiation of multipotent stem/stromal cells (MSCs). *In vivo* characterisation of immune cell subsets following scaffold implantation into a large bone defect demonstrated that AC-ECM drives an M2 macrophage phenotype, while GP-ECM containing scaffolds promoted a hybrid M1-M2 phenotype and enhanced vascularisation and vessel maturation. This distinct response to the implantation of GP-ECM containing scaffolds was associated with increased $CD45^+$ leukocyte and $CD3^+$ T cell infiltration, accompanied by elevated concentrations of IFN-γ and IL-17. Taken together this work demonstrates that the source tissue of ECM scaffolds plays a key role in regulating the phenotype of both macrophages and skeletal stem cells. Furthermore, these ECMs can direct the cellular differentiation and production of growth factors essential for the regeneration of their source tissue. This work highlights the need for a more thorough characterisation of innate immune cell subsets post-biomaterial implantation.

1. Introduction

Engineering an appropriate immune response is now recognised as a key consideration in the design of biomaterial scaffolds for tissue regeneration. A major determinant of downstream functional remodelling post biomaterial implantation is the early innate immune response, in particular that mediated by different macrophage phenotypes, which can predict success or failure of implant integration and tissue remodelling.[1–3] Macrophages are a primary effector cell of the innate immune system and are commonly targeted in regenerative medicine strategies due to their plasticity and diverse roles in the regeneration of damaged tissue.[4] Several *in vivo* models have supported the central role of macrophages in the normal tissue regeneration process; inferior healing was observed in animals depleted of macrophages.[5,6] Macrophages are an

* Corresponding author. Trinity Centre for Biomedical Engineering, Trinity Biomedical Sciences Institute, Trinity College Dublin, Dublin, Ireland.
E-mail addresses: olmahon@tcd.ie (O.R. Mahon), kellyd9@tcd.ie (D.J. Kelly).
[1] These authors contributed equally.

https://doi.org/10.1016/j.regen.2021.100041
Received 6 February 2021; Accepted 9 March 2021
Available online 29 March 2021

extremely plastic cell population and it is now well accepted that a temporal switch of macrophages from a classically activated 'M1' or pro-inflammatory state to alternatively activated 'M2' anti-inflammatory macrophages is associated with improved tissue healing. Higher ratios of M2/M1 polarized macrophages is associated with reduced fibrosis and scarring following injury.[1,2,7,8] While the M1/M2 paradigm is very useful, it is an oversimplification of the situation *in vivo*; in reality any individual cell is capable of expressing multiple aspects of either M1 or M2 phenotypes and can exist as transitional or hybrid phenotypes within this spectrum.[9]

The extracellular matrix (ECM) is a complex 3D network that provides both structural/physical support and biochemical signals to cells within a tissue. The ECM itself is composed of proteins and biomolecules deposited by the resident cells of each unique tissue and organ and these proteins can provide cues and biochemical signals that influence cell proliferation and differentiation under normal homeostatic conditions.[10] ECMs contain growth factors that promote tissue repair and remodelling which renders them very attractive biomaterials for tissue-specific regeneration applications. ECM-derived biomaterials can be generated from various tissue sources such as small intestine, urinary bladder, oesophagus, skeletal muscle and liver among others.[11,12] A key step in the development of such implants is decellularization of ECM, which involves removal of whole cells and nuclear material that would otherwise lead to adverse immunogenic effects. Inefficient decellularization results in xenogeneic cellular components and DNA remaining in the ECM, which can lead to adverse inflammatory responses and inhibition of appropriate constructive remodelling.[2,13] In contrast, appropriately decellularized ECM derived scaffolds have generally been associated with an M2-like host response and constructive remodelling at the tissue site.[2,3,14]

ECM derived scaffolds can therefore function as both a physical framework for endogenous/exogenous cells and as source of instructive biochemical signals that regulate numerous cellular activities and facilitate tissue regeneration. Such ECM biomaterial scaffolds have been used for preclinical studies and for clinical applications in humans.[15,16] Interestingly, ECM based materials have been shown to possess intrinsic capacity to polarize M2-type macrophages, and their degradation products can directly promote macrophage polarization and constructive remodelling.[1,3,17] Furthermore, we and others have demonstrated that musculoskeletal derived ECM scaffolds, such as articular cartilage (AC) and growth plate (GP), are capable of directing tissue specific cell differentiation and tissue repair for cartilage and bone regeneration respectively.[12,16,18] However, the ability of these distinct ECMs to differentially influence macrophage phenotype and immune cell function has not yet been determined in primary human macrophages. Given the phenotypic heterogeneity of macrophage polarization states and the diverse protein compositions of ECM based materials, further study of the exact phenotypes induced by diverse ECMs is required. It is likely that cell interactions with different ECMs will produce distinct macrophage phenotypes.

The overall objective of this study was to elucidate the primary phenotype of human macrophage and multipotent stem/stromal cells (MSC) upon exposure to ECM biomaterials derived from different musculoskeletal tissue sources. We demonstrate that articular cartilage (AC) derived ECM drives an M2-like phenotype in primary human macrophages, while growth plate (GP) derived ECM promotes a hybrid M1-M2 phenotype. Furthermore, GP-ECM appears to induce production of cytokines and growth factors that may be important for promoting vascularisation and bone formation. Specifically, TNF, IL-6, VEGF and Ang1, all of which have been shown to play important roles in the homeostasis and regeneration of functional bone tissue, were upregulated in the presence of GP-ECM. Moreover, these ECMs were found to direct differentiation of stem cells into cartilage like or bone like cells, providing further evidence that they possess intrinsic cues and factors that drive cellular differentiation associated with their source tissue. Lastly, we show that when implanted into a rat femoral defect model, GP-ECM containing scaffolds induce a hybrid M1-M2 phenotype in host macrophages and enhance vascularisation of the defect site, suggesting a potential new role for hybrid macrophage phenotype in vascular responses during biomaterial mediated bone repair. Taken together, this study demonstrates the importance of considering the ECM tissue source and its inherent immunomodulatory capacities in the design of ECM based scaffolds for tissue engineering and regenerative medicine.

2. Materials and methods

2.1. Study design

This study was designed to examine the role of the ECM isolated from different tissue sources on human macrophage and MSC phenotype. The use of human blood samples for this study was approved by the research ethics committee of the School of Biochemistry and Immunology, Trinity College Dublin and was conducted in accordance with the Declaration of Helsinki. Leukocyte-enriched buffy coats from anonymous healthy donors were obtained with permission from the Irish Blood Transfusion Service (IBTS), St. James's Hospital, Dublin. Donors provided informed written consent to the IBTS for their blood to be used for research purposes. All animal experiments were conducted in accordance with the recommendations and guidelines of The Health Products Regulatory Authority, the competent authority in Ireland responsible for the implementation of Directive 2010/63/EU on the protection of animals used for scientific purposes in accordance with the requirements of the Statutory Instrument No. 543 of 2012. Animal experiments were carried out under license (AE 19136/P069) approved by The Health Products Regulatory Authority and in accordance with protocols approved by Trinity College Dublin Animal Research Ethics Committee. The *n* for rodent models was based on the predicted variance in the model and was powered to detect 0.05 significance. Animals were randomly assigned to experimental groups before surgical procedure.

2.2. ECM solubilisation

Ligament (LIG), articular cartilage (AC) and growth plate (GP) used in the fabrication of ECM-derived scaffolds were harvested from the stifle joints of female pigs (4 months old) shortly after sacrifice. Pigs were obtained from a local abattoir. For tissue harvest the stifle joint capsules were opened, for the LIG tissue, the anterior cruciate ligaments were harvested and diced into 1 mm^3 pieces. The AC was obtained using a biopsy punch (8 mm) to shave off the articular cartilage from the femoral condyles. Following this, the head of the bone was sawed in half and hammered through the epiphyseal line to gain access to the growth plate cartilage which was then removed. Tissue solubilisation was then performed as previously described.[19] Briefly, tissue was pre-treated with 0.2 M NaOH, solubilised with pepsin (1500 U/ml) and the collagen was precipitated with NaCl (at a final concentration of 0.8 M for LIG, 0.9 M for AC and 2.5 M for GP).[20] The collagen pellet was resuspended in 0.5 M acetic acid followed by rotation at 4 RPM overnight at room temperature to fully dissolve the collagen into suspension. The salt precipitation procedure was then repeated a second time. The acid solubilised ECM was dialysed against 0.02 M Na_2HPO_4 for 48 h at 4 °C before being freeze dried.

2.3. Scaffold fabrication

Scaffolds were fabricated as previously described.[19] Briefly, lyophilized ECM was resuspended in DMEM (Gibco) and dissolved in 0.02 M acetic acid to give a final concentration of 10 mg/ml. Before the slurry was neutralised by adding 20 μl volumes of 0.1 M NaOH prior to chemical crosslinking using glyoxal (Sigma) at a final concentration of 5 mM for 30 min at 37 °C. The solution was then transferred to custom made moulds (height 5 mm and diameter 3 mm) and freeze dried (FreeZone Triad, Labconco, KC, USA). Scaffolds were subsequently

physically crosslinked in a vacuum oven (VD23, Binder, Germany) by dehydrothermal (DHT) treatment at 115 °C for 24 h at 0.2 mBar. Scaffold pore size was determined using SEM imaging as follows: SEM images were obtained using a Zeiss Ultra Plus (Zeiss, Germany) with an acceleration voltage of 5 kV and working distance of 5 mm. To quantify the mean pore size of the various scaffolds, 3 images (containing a minimum of 100 pores) from 3 different scaffolds were measured using imageJ.

2.4. Isolation and expansion of human bone marrow and infrapatellar fat pad derived stem/stromal cells

To isolate bone marrow derived multipotent stem/stromal cells (BM-MSCs), bone marrow aspirates (Lonza) were washed in PBS and centrifuged at 900×*g* for 10 min, supernatant was gently aspirated and cells were plated at 40–60 × 10^6/T175 (4000–5000 MSCs/cm^2). Ethical approval for the donation of human infrapatellar fat pad (IFP) tissue and subsequent isolation of fat pad stromal cells (FPSCs) from the tissue was obtained from the institutional review board of the Mater Misericordae University Hospital Dublin. Infrapatellar fat pad derived stem/stromal cells (FPSCs) were isolated as previously described.[19] BM-MSCs and FPSCs were expanded in DMEM supplemented with 10% FBS (Gibco), Penicillin (100 U/ml) and streptomycin (100 μg/ml) (Gibco) and 5 ng/ml fibroblast growth factor-2 (FGF-2, PeproTech). Expansion media was changed three times per week. BM-MSCs and FPSCs were not used beyond passage 3 for subsequent differentiation experiments.

2.5. Human blood monocyte-derived macrophages

Peripheral blood mononuclear cells (PBMC) were purified by density gradient centrifugation from leukocyte-enriched buffy coats from anonymous healthy donors, obtained with permission from the Irish Blood Transfusion Board, St. James's Hospital, Dublin. $CD14^+$ cells were positively selected using antiCD14 magnetic beads (eBiosciences) as previously described[21,22] and shown to be >90% pure, as determined by flow cytometry. Cells were cultured at 1 × 10^6 cells/ml for 6 days in RPMI 1640 medium supplemented with 1% penicillin-streptomycin and 10% Foetal Bovine Serum. Macrophage were differentiated by adding *M*-CSF (50 ng/ml) to the cultures on days 0 and 3. >95% of cells were $CD14^+CD11b^+$ as determined by flow cytometry (Fig. S1 A).

2.6. Culture of human macrophages with solubilised ECM

For immunocytochemistry, DQ-ova antigen uptake and surface marker flow cytometry experiments, primary human macrophages (1 × 10^6 cells/ml) were stimulated with a suspension of LIG-, AC- or GP-ECM (200 μg/ml) for 24 h. Alternatively for ELISAs and qRT-PCR experiments primary human macrophages (0.5 × 10^6 cells/scaffold) were seeded onto ECM scaffolds, allowed to adhere for 1 h, and then cultured for 24 h in complete RPMI. Supernatants were then harvested for cytokine analysis and cells were lysed for RNA extraction and gene expression analysis.

2.7. Biochemical/histological analysis of scaffolds and cell seeded constructs

Cell free scaffolds (Day 0) and FPSC/BM-MCS seeded constructs (Day 28) were analyzed for DNA, sulfated glycosaminoglycan (sGAG) and calcium content. sGAG quantification was performed using a 1, 9 dimethylmethylene blue (DMMB) assay according to the manufacturer's protocol with bovine tracheal chondroitin 4- sulfate used as a reference standard (Blyscan sulfated sGAG assay kit, Biocolor, Northern Ireland). Quantification of dsDNA in the digested constructs was performed using a Quant-iT Pico Green dsDNA kit (Invitrogen) according to the manufacturer's protocol. The combination of results from the DMMB and pico-green assays provides a ratio of sGAG normalized to dsDNA content. Calcium content was determined by an O-cresolphthalein complexone assay (Sentinel Diagnostics) according to the manufacturer's instructions. For histological analysis, samples were washed in PBS followed by overnight fixation in 4% paraformaldehyde (Sigma). Samples were dehydrated and wax embedded. Embedded constructs were then sectioned at a thickness of 5 μm using a microtome. Sections were stained with 1% alcian blue 8X in 0.1 M HCl to examine sGAG, picrosirius red to examine total collagen deposition and 2% alizarin red to examine mineral deposition. To identify the specific collagen types present in the constructs, immunohistochemistry was performed for collagen type I, type II or X (all Abcam antibodies) as previously described.[19]

2.8. Mechanical testing

Scaffolds (Φ5 mm x h 3 mm) were subjected to a uniaxial unconfined compression test in PBS using a single column mechanical tester (Zwick/Roell Z2.5, Herefordshire, UK) with a 5 N load cell. To obtain the equilibrium modulus of cell-free scaffolds, stress relaxation tests were performed whereby 20% strain was applied followed by relaxation until equilibrium was achieved.

2.9. Assessment of endotoxin contamination

Prior to culture with primary human macrophages, AC, LIG and GP derived solubilised ECM preparations were first tested for lipopolysaccharide (LPS) contamination using the HEK-Blue™ hTLR4 assay system (Invivogen). HEK-blue cells (5 × 10^5 cells/ml) expressing TLR4 were stimulated with LPS (10–200 ng/ml; positive control), AC, LIG or GP scaffolds for 24 h. The expression of SEAP which is under the control of NF-kB and AP-1 was tested by incubating cell supernatants with HEK-blue detection medium for 30 min at 37 °C and absorbance was read at 650 nm.

2.10. Seeding LIG, AC and GP scaffolds with BM-MSCs or FPSCs for differentiation studies

To assess the capacity of the different scaffolds to support chondrogenic differentiation they were seeded with FPSCs, while to examine the capacity of the scaffolds to support osteogenic differentiation they were seeded with BM-MSCs. Cell seeding was performed as previously described.[19] Briefly, 0.5 × 10^6 FPSCs or BM-MSCs were seeded onto individual scaffolds suspended in 25 μl of expansion media. Cells were allowed to attach to the scaffolds for 1 h in an incubator at 37 °C. After cell attachment, to examine chondrogenesis; 2.5 ml of chemically defined chondrogenic differentiation media (CDM) was added per FPSC seeded scaffold in 12 well plate. CDM consisted of high glucose DMEM supplemented with Penicillin (100 U/ml) and streptomycin (100 μg/ml) (both Gibco), 100 μg/ml sodium pyruvate (Sigma), 40 μg/ml L-Proline (Sigma), 50 μg/ml L-ascorbic acid-2-phosphate (Sigma), 1.5 mg/ml bovine serum albumin (BSA-Sigma), 1X insulin transferrin selenium (ITS-Gibco), 100 nM dexamethasone (Sigma) and 10 ng/ml transforming growth factor beta-3 (TGF-β3 – PeproTech). To examine osteogenesis; 2.5 ml of osteogenic differentiation media (ODM) was added per BM-MSC seeded scaffold in 12 well plate. OSM consisted of high glucose DMEM supplemented with Penicillin (100 U/ml), streptomycin (100 μg/ml), 10 mM βGlycerol Phosphate, 0.05 mM L-ascorbic acid-2-phosphate (Sigma) and 100 nM dexamethasone (Sigma). The cell seeded constructs were maintained in CDM/OSM for 28 days with the media being replenished three times per week.

2.11. Enzyme-linked immunosorbent assay

Supernatants from macrophages were collected 24 h after treatment and cytokine concentrations of IL-12, TNF, IL-6, IL-8 and IL-10 was analyzed. Protein secretion was measured using commercially available

ELISA kits (eBiosciences) according to manufacturer's instructions.

2.12. Real-time polymerase chain reaction (PCR)

RNA from macrophages was extracted using High Pure RNA Isolation Kits (Roche, Basel, Switzerland) and assessed for concentration and purity using the NanoDrop 2000c UVis spectrophotometer. RNA was equalized and reverse transcribed using the Applied Biosystems High-Capacity cDNA reverse transcription kit. Real-time PCR was carried out on triplicate cDNA samples with the use of the CFX96 Touch Real-Time PCR Detection System (Bio-Rad Laboratories, California). Real-time PCR for the detection of *CXCL9, CXCL10, CCL13* and *MRC1* mRNA was performed using the TaqMan fast universal PCR Master Mix (Applied Biosystems) and predesigned TaqMan gene expression primers. mRNA amounts were normalized relative to the housekeeping gene Ribosomal Protein 18s. For assessment of growth factor gene expression Sigma primers for *VEGF, Ang1* and *FGF2* (Supplementary Table 1) were used and mRNA amounts were normalized to *GAPDH* as housekeeping gene.

2.13. Assessment of macrophage surface marker expression and phagocytic capacity

Macrophages were fixed with 4% PFA, incubated in Block and Perm solution (3% BSA with 0.1% Triton X) for 1 h at room temperature. Cells were then incubated in primary antibodies specific for CD206, CD163 or CD80 (1:1000 dilution for CD206 and 1:500 dilution for CD163 and CD80) overnight at 4 °C. Cells were washed and incubated in secondary antibodies for 1 h at room temperature (anti-rabbit Alexa Fluor 488 for CD206 and CD163, and anti-rabbit Alexa Fluor 647 CD80 (all 1:1000). Cells were washed and counterstained with DAPI (1 mg/ml) for 15 min and imaged using a Leica SP8 scanning confocal microscope.

Alternatively, surface marker expression was assessed by flow cytometry. Macrophages were Fc blocked for 15 min prior to staining with fluorochrome conjugated antibodies specific for CD14, CD11b, CD40 and CD86 (M1), CD163 and CD206 (M2), fixed with 4% PFA washed and acquired on a FACSCanto™ II (BD Biosciences) and analyzed by flow cytometry. Compensation beads singly stained with every fluor channel utilized were acquired to adjust for spectral overlap. An unstained sample was also run as a control. (Supplementary Table 2 for antibody dilutions and fluorophores).

For assessment of phagocytosis or antigen uptake, DQ-Ova was prepared to a stock concentration of 1 mg/ml. Cells were incubated with fresh medium containing 500 ng/ml DQ-Ova for 20 min at 37 °C, followed by an incubation at 4 °C for 10 min. Cells were then washed in PBS, centrifuged at 300×*g*, re-suspended in PBS and immediately acquired using FACSCanto™ II (BD Biosciences). Cells treated with media containing no DQ-Ova were used as a gating control for DQ-Ova positive cells.

2.14. Surgical implantation of ECM scaffolds into rat femoral defect

Critically-sized (5 mm) femoral defects were created in immune-competent adult Fischer rats (>12 weeks old) following an established procedure.[23] Constructs were press-fit into the defect site and repair tissue was harvested for analysis at 1 week post-implantation. One defect was created per animal and n = 5–8 constructs were implanted per time point. Briefly, anaesthesia was induced and maintained by isoflurane-oxygen throughout the surgery. The rats were also injected with buprenorphine to provide pain relief during and after surgery. The shaft of the left femur was exposed by dissections and the periosteum was scraped back to allow access to the bone. A weight-bearing polyetheretherketone (PEEK) internal fixation plate was secured to the exposed femur with four screws into pre-drilled holes. A 5 mm mid-diaphyseal defect was then created using a dental drill fitted with 2 small circular parallel saw blades welded to a narrow straight rod separated with a 5 mm spacer. The defect site was thoroughly irrigated with saline to remove bone debris before it was treated with a construct. The wounds were closed with sutures and the rats were allowed to recover. On dates of scheduled explant retrieval, rats were sacrificed by CO_2 asphyxiation and cervical dislocation. The repaired femur, with the PEEK plate fixator intact, was carefully separated from the adjacent hip and knee joints for analysis.

2.15. Characterisation of immune response and macrophage phenotype in rat femoral defect model

Punch biopsies (4 mm) of the defect site were performed 1 week post-surgery and cells were recovered by digestion in a Collagenase digestion cocktail (Collagenase VI (2 mg/ml), DNAse I (0.1 mg/ml) and Hyaluronidase (0.5 mg/ml) for 45 min at 37 °C and 255 rpm. Cells were blocked by incubating in Fcγ blocker (BD Pharmingen; 1 μg/ml) for 10 min. To discriminate live from dead cells, cells were stained with LIVE/DEAD Aqua for an additional 30 min. Staining was performed with fluorescent Abs directed against CD11b, CD3, Ly6G, CCR2, CX3CR1, CD19, F4/80, Siglec F, CD45, MHCII, and CD86 (Supplementary Table 3). Cells were acquired using LSRFortessa (BD). Analysis was completed using FlowJo version 9.2 (Tree Star). Gating strategies utilized in all experiments are detailed as previously described.[23]

In order to assess circulating cytokines 1 week post-surgery, cardiac punctures were performed and blood samples were centrifugated at 300×*g* for 20 min and serum was collected. IL-5, IL-10, IL-17 and IFN-γ cytokine concentrations were quantified by ELISA (R&D systems) according to manufacturer's instructions.

2.16. Histological and immunohistochemical analysis

Tissue samples were fixed in 4% paraformaldehyde, decalcified in EDTA for 1 week, dehydrated, and embedded in paraffin-wax using an automatic tissue processor (Leica ASP300). All samples were sectioned with a thickness of 10 μm using a rotary microtome (Leica Microtome RM2235) and affixed to microscope slides. Sections were stained with haematoxylin and eosin (H&E) to assess tissue architecture and vessels and imaged using Aperio Scanscope slide scanner. Quantitative analysis was performed on multiple H&E-stained slices, whereby total number of vessels in a ROI of 2 × 2 mm were counted using the count function on Image J. Vessel number was averaged from 2 stained tissue slices per rat for every experimental group (n = 4 rats).

Immunofluorescence analysis was used to detect von Willibrand factor (vWF) and α -smooth muscle actin (α-SMA). Sections were deparaffinised and rehydrated in varying ethanol grades (100-50%). Antigen retrieval was then performed by incubating sections in proteinase K (20 min at 37 °C) in a humidified chamber. Slides were washed with 0.5% (v/v) PBS-Tween and blocked (blocking diluent, BD, 3% donkey serum, 1% BSA in PBS) for 1 h at room temperature. Slides were incubated in primary antibody overnight at 4 °C with goat polyclonal α-SMA in diluent (ab21027; Abcam, 1:250) washed three times with 1% BSA in PBS prior to incubation with donkey anti-goat Alexa Fluor 488 (ab150129; Abcam, 1:200) for 1 h at room temperature. Samples were washed three times in PBS with 1% w/v BSA and slides were incubated overnight at 4 °C with rabbit polyclonal vWF antibody (ab6994; Abcam, 1 : 200) in PBS with 3% donkey serum (w/v) and 1% BSA. Slides were washed three times in PBS with 1% w/v BSA, and sections were incubated Alexa Fluor® 647 donkey anti-rabbit secondary antibody (ab150075, Abcam, 1:200), for 1 h at room temperature in the dark. Slides were washed three times with 1% BSA in PBS, mounted with flouroshield mounting media with DAPI, dried and fluorescence emission was detected using a Leica SP8 scanning confocal microscope. Total number of single positive (vWF) and double positive (vWF/α-SMA) vessels was quantified using the count function on Image J (determined across 10 fluorescent images per rat (n = 3 rats)) and the ratio of single positive to double positive vessels was used as an indication of vessel

maturity.

Immunofluorescence analysis was used to detect the pan macrophage marker CD68, the M2 marker CD206 and the M1 marker CD80. Sections were deparaffinised and rehydrated in varying ethanol grades (100-50%). Heat mediated antigen retrieval with Sodium Citrate buffer (10 mM Sodium Citrate, 0.05% Tween 20, pH 6.0) for 20 min in a microwave pressure cooker. Slides were allowed to cool for 15 min and washed three times in PBS. Sections blocked (3% serum (donkey & goat), 0.1% Triton X 100, 0.05%Tween 20, 1% BSA in PBS) for 1 h at room temperature. All slides were stained and incubated in primary antibodies overnight 4 °C with mouse monoclonal CD68 (ab955; Abcam, 1:200) as a pan macrophage marker. At the same time, sections were either dual stained with rabbit polyclonal CD206 (ab64693; Abcam, 1:100) to identify M2 macrophages or with rabbit polyclonal CD80 (ab215166; Abcam, 1:200) to identify M1 macrophages. Sections were then washed with 0.5% (v/v) PBS-Tween prior to incubation with donkey anti-rabbit Alexa Fluor 488 for CD206 and CD80 (ab150073; Abcam, 1:300) and goat anti-mouse Alexa Fluor 647 for CD68 (ab150115; Abcam, 1:200) for 1 h. Slides were washed with 0.5% (v/v) PBS-Tween, mounted with flouroshield mounting media, dried and fluorescence emission was detected using a Leica SP8 scanning confocal microscope.

2.17. In vivo μCT analysis

μCT scans were performed on constructs using a Scanco Medical vivaCT 80 system (Scanco Medical, Bassersdorf, Switzerland). Rats (n = 8) were scanned at 4 weeks post-surgery to assess defect bridging and bone formation within the defect. First, anaesthesia was induced in an induction chamber. Next, the rats were placed inside the vivaCT scanner and anaesthesia was maintained by isoflurane-oxygen throughout the scan. Next, a radiographic scan of the whole animal was used to isolate the rat femur. The animal's femur was aligned parallel to the scanning field-of view to simplify the bone volume assessments. Scans were performed using a voltage of 70 kVp, and a current of 114 mA. A Gaussian filter (sigma = 0.8, support = 1) was used to suppress noise and a global threshold of 210 corresponding to a density of 399.5 mg hydroxyapatite/cm^3 was applied. A voxel resolution of 35 μm was used throughout. 3D evaluation was carried out on the segmented images to determine bone volume and density and to reconstruct a 3D image. Bone volume and bone density in the defects was quantified by measuring the total quantity of mineral in the central 130 slices of the defect. The variance of bone density with depth through the constructs was analyzed qualitatively by examining sections at a depth of 25%, 50% and 75% from the top of the construct (one quarter, mid and three-quarter sections). The bone volume and densities were then quantified using scripts provided by Scanco.

2.18. Statistical analysis

GraphPad Prism 8.00 (GraphPad Software) was used for statistical analysis. A one-way ANOVA or Kruskal-Wallis test were used for the comparison of more than two groups for parametric and non-parametric analysis respectively, with the Tukey or Dunns test for multiple comparisons. P values of <0.05 were considered significant and denoted with an asterisk. Normality tests were carried out to ensure that the data was normally distributed for parametric statistical tests.

3. Results

3.1. Characterisation of ECM scaffolds derived from different musculoskeletal tissues

In order to isolate ECM material from different musculoskeletal tissues, porcine growth plate (GP), articular cartilage (AC) and ligament (LIG) were subjected to a collagen solubilisation protocol as previously described.[19] Scaffolds were then fabricated from these ECMs (Fig. 1 A) and the mechanical properties, porosity and pore size of each scaffold type assessed. Post fabrication all scaffolds displayed highly elastic mechanical properties when manually compressed (Fig. 1 A), returning to near their original shape after unloading. Given that scaffold pore size and mechanical properties can greatly influence cellular response and behaviour, we assessed the physical and mechanical properties of the scaffolds. SEM imaging and pore size analysis revealed that all scaffolds had a relatively homogenous pore architecture and comparable pore sizes ranging from approximately 20-40 μm (Fig. 1 A & B). The equilibrium moduli of all scaffolds was in the range of 0.5–0.8 kPa, with no significant difference across the groups (Fig. 1C), demonstrating that all ECM scaffold types, regardless of their tissue source displayed similar physical properties. Biochemical analysis revealed near complete removal of sGAG from the matrix in all groups, furthermore, all ECM scaffolds contained approximately 50 ng/mg or below of DNA, demonstrating effective decellularization (Fig. 1 D & E). Moreover, the concentration of contaminating endotoxin (LPS) was below the threshold level for TLR4 activation (Fig. 1 F), verifying that there was no LPS contamination in the ECM preparations prior to culture with macrophages.

3.2. Solubilised ECM from differential tissue sources differentially influence macrophage phenotype

It has previously been demonstrated that ECM can drive an M2-like phenotype in both murine and human macrophages.[3,24] In order to investigate whether solubilised ECM from different musculoskeletal sources modulated macrophage phenotype, primary human macrophages were isolated as previously described[21] and differentiated into $CD14^+CD11b^+$ macrophages (Fig. S1 A). Cells were stimulated with LIG, AC or GP derived ECM and the expression of surface markers associated with M1 or M2-type macrophages was assessed using immunofluorescent staining. Importantly, treatment of macrophages with all ECM types did not affect cell viability after 24 h (Fig. S1 B). Cells treated with IFN-γ (20 ng/ml) were included as positive controls for M1 macrophages, while cells treated with IL-4 (20 ng/ml) were included as a positive control M2 macrophages. As expected, IL-4 stimulated cells exhibited intense fluorescence for CD206 and CD163 compared to untreated control cells. Macrophages stimulated with AC and GP also staining highly positively for both of these markers. In contrast, LIG-treated cells exhibited no positive staining for either of these markers. Interestingly macrophages exposed to GP, but not AC, stained for CD80 to a near comparable level to that of the M1 positive control, IFN-γ (Fig. 2 A).

In order to assess whether changes in M1-like and M2-like markers occurred in a 3D system, macrophages were seeded onto ECM derived scaffolds and their phenotype assessed by RT-PCR. In line with the immunocytochemistry data, AC and GP, but not LIG, significantly upregulated mRNA expression of the M2 associated genes *Mrc1* (codes for CD206) and *CCL13* compared to that of control cells. Interestingly, only GP-ECM induced robust expression of the M1 associated genes *CXCL9* and *CXCL10*, which encode for chemokines that are primarily involved in the chemotaxis and recruitment of T cells[25,26] (Fig. 2 B). This suggests that distinct macrophage phenotypes are induced by ECMs sourced from different tissues, with AC-derived ECM primarily driving an M2-like phenotype and GP-derived ECM inducing an M1/M2 hybrid phenotype.

3.3. ECM derived from different sources induces functionally distinct macrophage responses

In order to further validate the findings and to more extensively characterise the functionality of these macrophages, cytokine and growth factor induction was assessed by ELISA and RT-PCR respectively. GP- but not AC-derived ECM induced IL-6 and TNF production, which have a known pro-osteogenic role,[27–29] while none of the ECM types

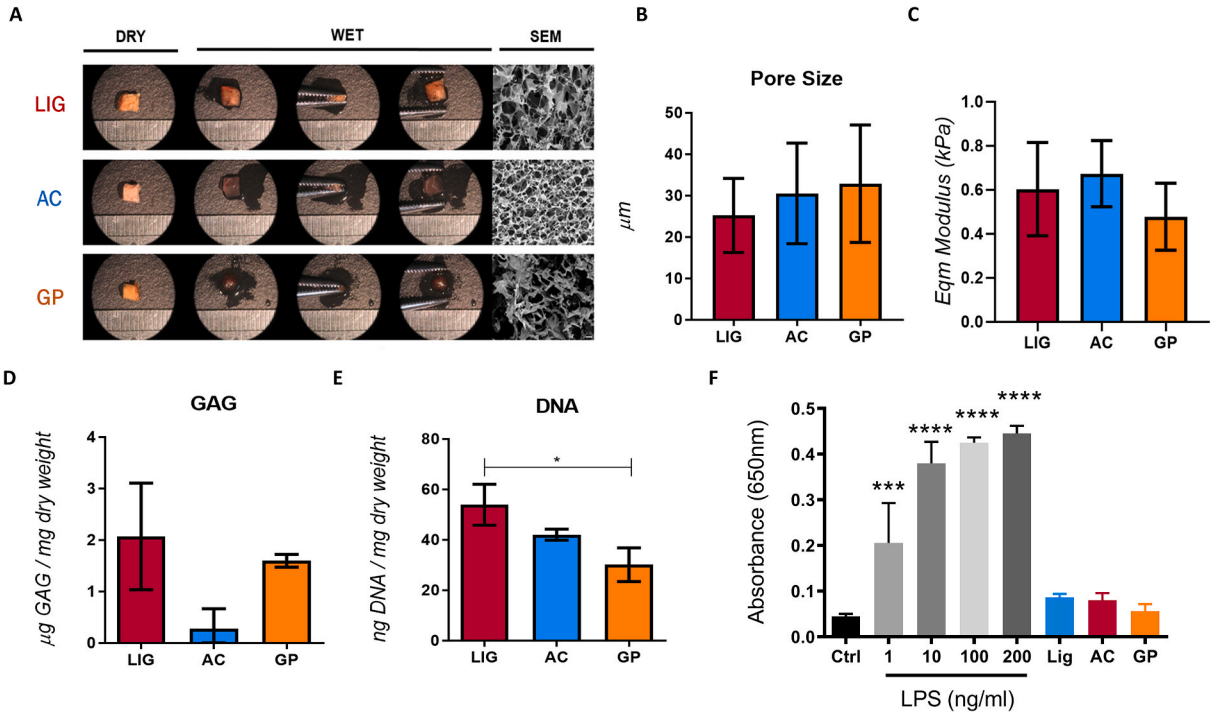

Fig. 1. Characterisation of musculoskeletal derived ECM. (A) Visualisation of the physical characteristics of the ECM scaffolds, obtained by stereoscopic photography and scanning electron microscopy (SEM-scale bar = 20 μm). **(B)** Mean pore diameter of scaffold was obtained from 3 scaffolds per group. **(C)** To obtain the cell free ECM scaffold equilibrium modulus, stress relaxation tests were performed whereby 20% strain was applied to the samples (n = 4). **(D)** sGAG (n = 3) and **(E)** DNA levels of scaffolds were quantified by biochemical assays (n = 3). For mechanical testing and biochemical assays, Data is represented as Means ± SD for ≥3 independent samples. Statistical differences were assessed using one-way ANOVA with Tukey post-test *$p < 0.05$. **(F)** ECM preparations were shown to be endotoxin free, using the HEK-Blue™ hTLR4 assay system (Invivogen). The expression of SEAP, as measured by absorbance at 650 nm, by ECM treated macrophages was comparable to untreated control cells. As a positive control, cells were treated with LPS (1, 10, 100 or 200 ng/ml). Data is represented as Means ± SEM for triplicate cultures of 3 independent donors. Statistical differences were assessed using one-way ANOVA with Tukey post-test. ***$p < 0.001$, ****$p < 0.0001$ vs untreated control.

induced IL-12 or IL-10 production. Interestingly, high levels of the chemokine IL-8 were observed in macrophages cultured in the presence of AC- or GP-derived ECM. While the precise role of this chemokine in chondrogenesis and osteogenesis has not yet been established, IL-8 in the presence of bone marrow concentrate enhances chondrogenic markers in MSCs, while IL-8 alone has also been shown to promote osteoclastogenesis.[30,31] Cytokine production was negligible in the presence of LIG-derived ECM (Fig. 3 A). In addition to altering cytokine production, AC and GP ECMs enhanced macrophage expression of growth factors known to be important in the maintenance and regeneration of the source tissue from which they are derived. AC-derived ECM specifically upregulated *FGF2*, a known pro-chondrogenic factor while only GP derived ECM was found to significantly upregulate mRNA expression of the pro-angiogenic factor *VEGF*.[32,33] No effect was observed on *ANG1* mRNA expression in the presence of LIG-derived ECM, however AC- and GP-derived ECMs enhanced expression of this growth factor, with robust and higher induction by GP-ECM. LIG did not influence growth factor induction in primary macrophages (Fig. 3 A).

Having demonstrated distinct macrophage phenotypes, the phagocytic capacity of macrophages was assessed as a measure of their functionality. It is well established that upon maturation macrophages reduce their phagocytic capacity, as their role switches from tissue surveillance to antigen presentation.[34] Furthermore, the phagocytic capacity of activated or M1-like macrophages has been shown to be much lower than that of resting or M2 macrophages.[21,35,36] In order to determine the phagocytic capacity of ECM-treated macrophages, cells were incubated with FITC-conjugated DQ-Ovalbumin (DQ-Ova; 500 ng/ml) post ECM-treatment and analyzed for antigen uptake by flow cytometry. In agreement with previous studies, unstimulated control macrophages displayed high DQ-Ova uptake, while M1 positive control cells stimulated with IFN-γ had reduced uptake. As expected, M2 positive control cells had significantly enhanced phagocytic capacity (Fig. S2). In addition, AC-ECM treated macrophages retained their high phagocytic capacity, which is consistent with the M2-like phenotype observed in earlier experiments. While GP-ECM treated scaffolds displayed comparable levels of M2-associated markers, high M1-associated markers were also observed, and interestingly, phagocytic capacity of GP-ECM treated cells was significantly reduced compared to that of untreated cells (Fig. 3 B & C). Taken together our findings suggest that while GP-ECM treated macrophages upregulate their M2 associated markers, they are also becoming more activated and losing their phagocytic capacity and exhibiting a distinct M1-M2 hybrid phenotype.

3.4. ECM scaffolds derived from different musculoskeletal tissues support distinct MSC phenotypes

We have previously demonstrated that AC-ECM derived scaffolds support the robust chondrogenic differentiation of infrapatellar fat pad derived stomal cells *in vitro* after the optimization of concentrations of both the ECM itself and the crosslinker.[19] However, the ability of solubilised ECM-based scaffolds fabricated from other tissues in supporting chondrogenesis remains unclear. To this end, 500,000 FPSCs, which have been shown to undergo robust chondrogenesis *in vitro*,[38] were seeded onto LIG, AC and GP scaffolds and cartilage matrix specific tissue deposition was assessed after 28 days in chondrogenic culture conditions. ECM-derived scaffolds fabricated from LIG-ECM, which has previously been shown to promote tenogenic responses in MSCs,[37] supported lower levels of (sGAG) deposition as demonstrated by alcian blue histological staining (Fig. 4 A) and biochemical quantification compared to scaffolds derived from type II collagen rich AC-ECM (Fig. 4

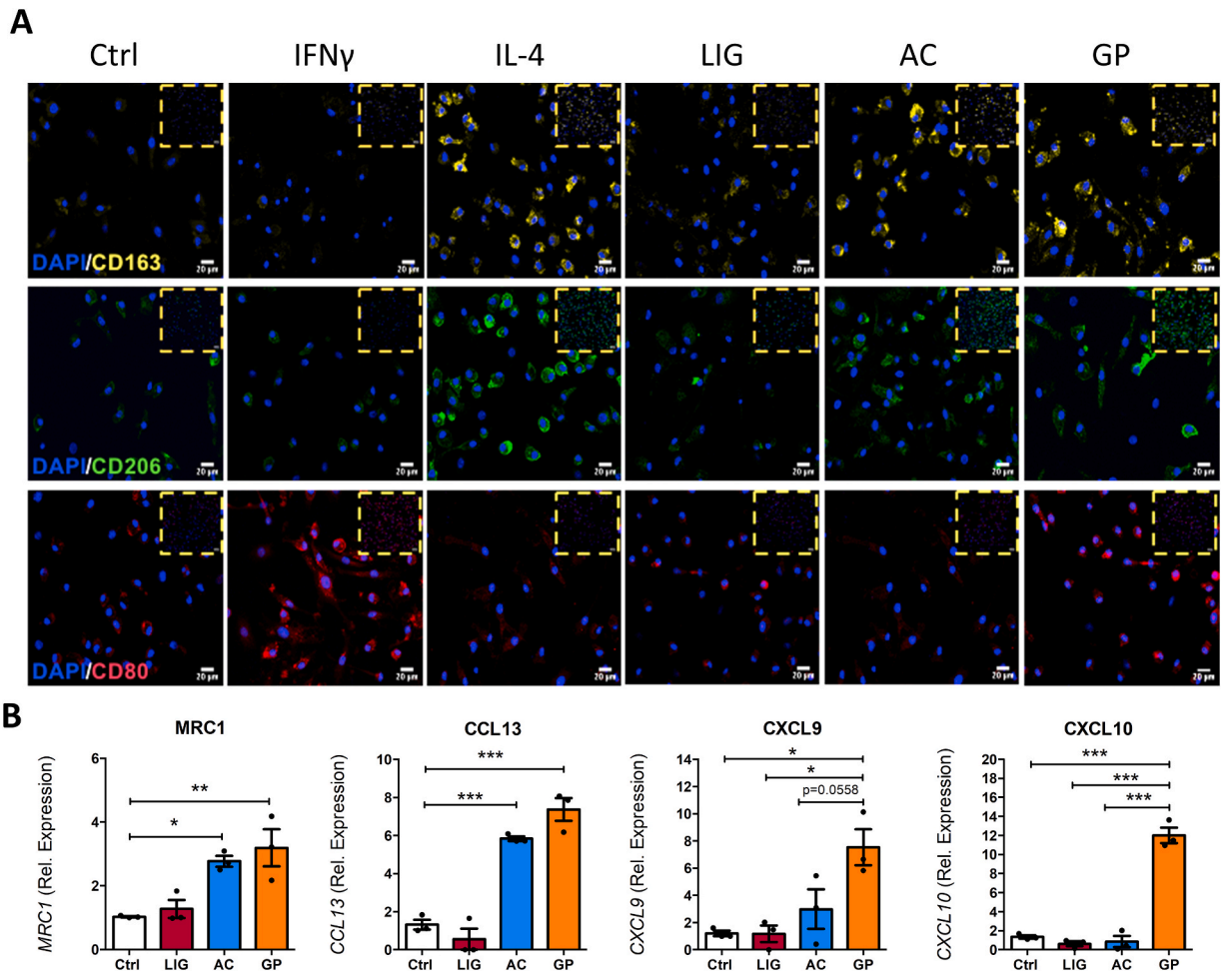

Fig. 2. ECM promote distinct macrophage phenotypes. (A) Primary human macrophages (1×10^6 cells/ml) were stimulated with either LIG-, AC- or GP-ECM (200 μg/ml) for 24 h. Alternatively, cells were stimulated with IFNγ (20 ng/ml) for an M1-like positive control, or IL-4 (20 ng/ml) for an M2-like positive control. Cells were fixed and immunolabelled for the M2 markers (CD163, CD206) or the M1 marker (CD80). Representative images of for each treatment group, CD163 (yellow), CD206 (green), DAPI (blue). Magnification = 20×. Scale bar = 50 μm. **(B)** Primary human macrophages (0.5×10^6 cells) were seeded onto ECM scaffolds for 24 h mRNA levels of *MRC1, CCL13, CXCL9* and *CXCL10* were analyzed by qRT-PCR. All data is represented as Means ± SEM for triplicate cultures of 3 independent donors. Statistical differences were assessed using one-way ANOVA with Tukey post-test. *$p < 0.05$, **$p < 0.01$, ***$p < 0.001$.

B) after 28 days of *in vitro* culture. This was also this case for ECM scaffolds derived from GP-ECM. While all three scaffold variants supported chondrogenic differentiation to some extent as evidenced by sGAG and type II collagen deposition, the most robust staining for both of these key chondrogenic markers was observed in the AC-ECM group. Upon quantification of DNA content of the scaffolds after 28 days, we observed a significant increase in DNA content in the GP scaffolds when compared to LIG and AC, indicating that the GP scaffolds continued to promote FPSC proliferation (Fig. 4C). Interestingly, under chondrogenic differentiation conditions neither the LIG-ECM, AC-ECM or GP-ECM scaffolds seemed to promote robust endochondral ossification or mineralization as demonstrated by the lack of positive collagen type X or alizarin red staining. When calcium content was quantified biochemically no differences were observed between the scaffold groups (Fig. 4 D).

Having established that AC-ECM scaffolds promoted the greatest levels of chondrogenic differentiation, we next sought to elucidate which of the scaffold variants supported robust osteogenic differentiation. BM-MSCs, which have been shown to possess good osteogenic capacity,[38] were seeded onto LIG, AC and GP scaffolds (500,000/scaffold) and maintained for 28 days in osteogenic medium. Interestingly, despite the potent osteogenic stimulus provided by the osteogenic medium, AC-ECM scaffolds were still able to promote the deposition of low levels of sGAG as evidenced by positive (albeit weak) staining for alcian blue (Fig. 5 A), with significantly more sGAG deposition observed compared to LIG-ECM scaffolds (Fig. 5 B). The GP derived scaffolds were observed to promote robust osteogenic differentiation of BM-MSCs, as observed by both the alizarin red staining for mineralization (Fig. 5 A) and the biochemical quantification of calcium in the constructs after 28 days of culture (Fig. 5 D). No positive alizarin red staining or quantified calcium was observed in the AC-ECM scaffolds, while the LIG-ECM scaffolds did support low levels of calcium deposition. Taken together, these differentiation experiments indicate that despite the physical similarities of the scaffolds, the ECM material used is a powerful stimulus to preferentially and specifically drive differentiation of adult stromal cell fate towards chondrogenic or osteogenic lineages. Specifically, that AC-ECM promotes chondrogenic differentiation and GP-ECM promotes osteogenesis.

3.5. *Implantation of GP:ECM containing scaffolds recruits CD45$^+$ leukocytes and T cells in a rat femoral defect*

We next sought to determine whether the phenotypic changes we observed *in vitro* with AC and GP ECM scaffolds translated into a physiologically relevant *in vivo* system, and therefore characterized immune responses to ECM scaffolds using a previously established rat femoral

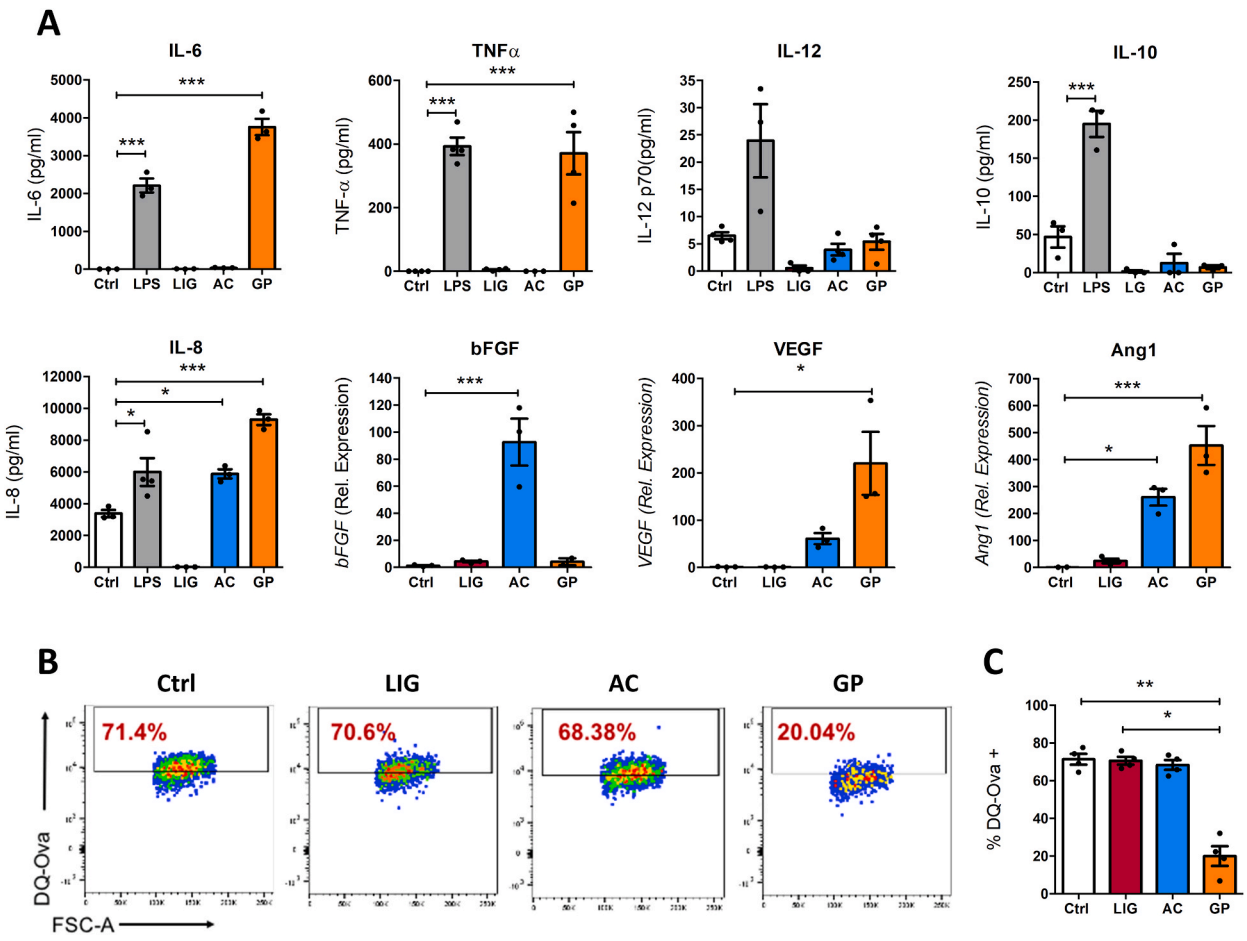

Fig. 3. GP and AC derived ECM alter macrophage functionality and secretome. (A) Primary human macrophages (1×10^5 cells) were seeded onto ECM scaffolds for 24 h. IL-6, TNF, IL-10, IL-12 and IL-8 cytokine production was quantified in cell supernatants by ELISA. mRNA levels of *FGF2, VEGF* and *Ang1* were analyzed by qRT-PCR. All data is represented as Mean ± SEM for triplicate cultures of 3–4 independent donors. Data was analyzed using Kruskal Wallis with Dunn's post-test for cytokine assays and one-way ANOVA with Tukey post-test for real-time PCR assays. **(B)** Macrophages were stimulated with ECM (200 μg/ml) for 24 h and then incubated with FITC-conjugated DQ-ovalbumin (DQ-Ova; 500 ng/ml) for 30 min prior to analysis by flow cytometry. Representative dot plots depicting DQ-Ova uptake by ECM treated macrophages. **(C)** Pooled data (n = 4) depicts percentage DQ-Ova uptake. All data is represented as Mean ± SEM and analyzed using Kruskal Wallis test with Dunn's post-test. *p < 0.05, **p < 0.01, ***p < 0.001.

defect model.[23] Somewhat unexpectedly, the GP-ECM scaffolds contracted and appeared to disintegrate in the presence of blood around the bone defect site (data not shown). Therefore, to create a more stable GP containing implant, a blended scaffold was fabricated using GP- and LIG-derived ECM at a 4:1 ratio. LIG-ECM was chosen for this purpose as we previously demonstrated it to be a relatively immunologically inert material *in vitro* and is more mechanically stable, likely due to its high levels of fibril type I collagen. We confirmed that this blended GP (GP:LIG) scaffold displayed comparable capacity to induce a M1-M2 hybrid macrophage phenotype observed with a GP-ECM only scaffold *in vitro* (Fig. S 3). These AC-ECM or GP:LIG-ECM scaffolds were then implanted into a 5 mm femoral defect and tissue was harvested for analysis 1 week post-implantation. Flow cytometric analysis of immune cell subsets at the defect site revealed significantly more $CD45^+$ leukocytes in rats implanted with GP:LIG-ECM scaffolds, compared to both empty defect and AC-ECM implants. Furthermore, significant infiltration of T cells ($CD45^+CD3^+CD19^-$) was present in GP:LIG-ECM scaffolds, but not with empty or AC-ECM scaffolds. Neutrophils ($CD45^+CD11b^+Ly6G^+$) were significantly higher following implantation of either scaffold, however this is not surprising as both AC-ECM and GP:LIG-ECM enhanced production of IL-8, a chemokine that mobilizes neutrophils, in earlier *in vitro* cultures (Fig. 6 A). There was no discernible difference in the absolute numbers of macrophages (Fig. 6 A) B cells ($CD45^+$ $CD19^+$ Siglec F^-) or eosinophils ($CD45^+$ $CD19^-$ Siglec F^+SSc^{high}) (Fig. S 4 A). Moreover, there was no significant difference in the number of infiltrating neutrophils, macrophages, B cells or eosinophils in tissue taken outside the defect area, however, significantly less T cells were present in the region outside the defect/implantation site in rats implanted with GP:LIG-ECM scaffolds (Fig. S 4 B), suggesting that T cells migrate from the outer region into the centre of the defect and the scaffold. Individual T cell subsets were not assessed as part of this study, however, serum cytokine analysis revealed higher concentrations of the Th2-associated cytokine, IL-5, in the AC-implanted rats. Conversely, circulating concentrations of the Th1-associated cytokine IFN-γ, and the Th17-derived cytokine IL-17 A, were significantly higher in rats implanted with the GP:LIG-ECM scaffolds compared with empty defect and significantly higher than the AC-ECM implanted rats, suggesting a role for Th1 or Th17 subsets of T cells. No difference in the Treg associated cytokine, IL-10 was observed, which was not surprising given the lack of induction of IL-10 in our *in vitro* cultures by either ECM scaffold (Fig. 6 B).

3.6. GP:LIG-ECM scaffolds induce a hybrid M1/M2 macrophage phenotype in vivo

Having observed distinct macrophage phenotypes upon culture with ECM *in vitro*, with AC-ECM driving a primarily M2-like phenotype and GP-ECM driving a hybrid M1/M2 phenotype, we next characterized the macrophage populations and phenotype *in vivo*. A significantly higher

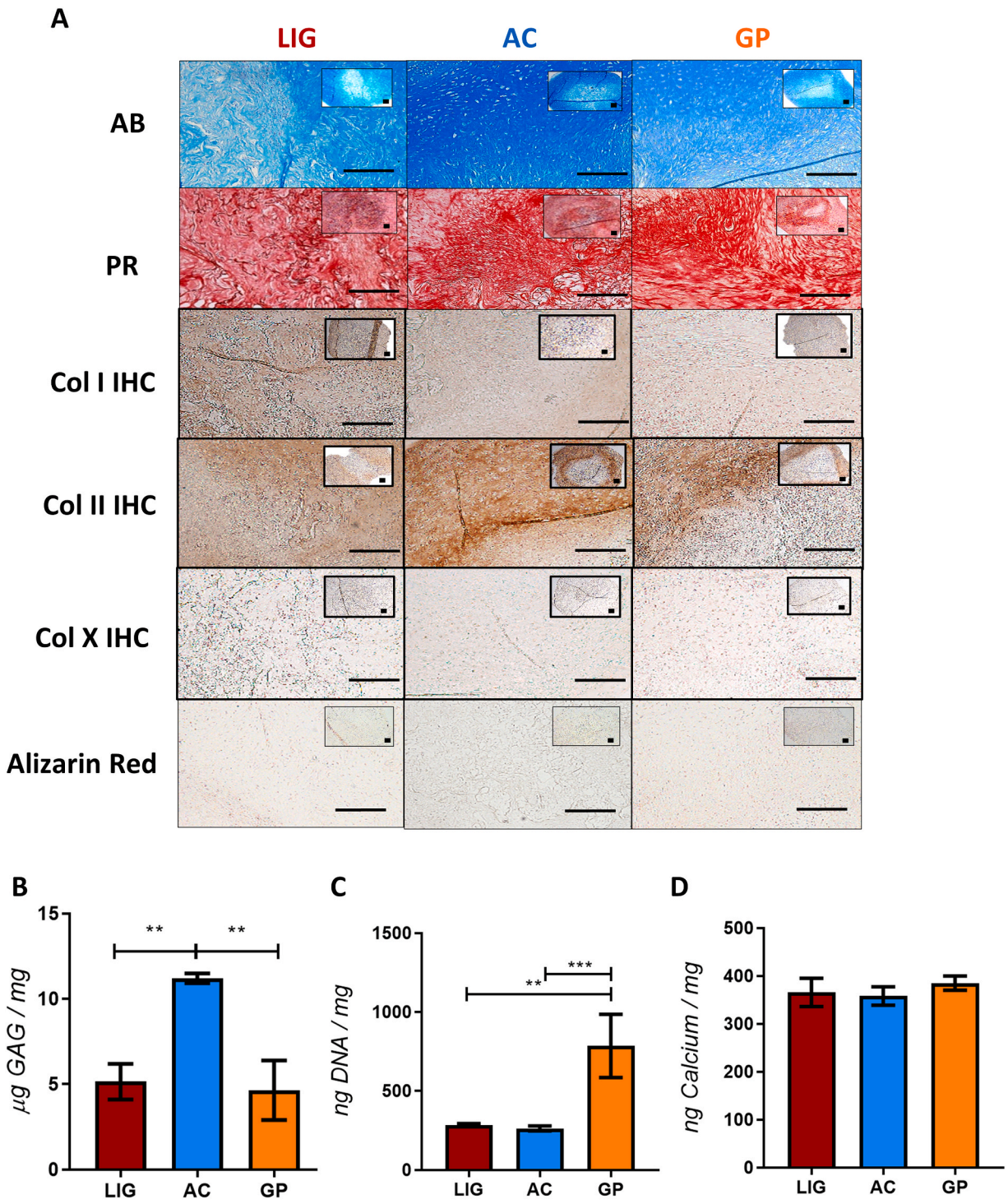

Fig. 4. AC-ECM scaffolds promote robust chondrogenic differentiation of FPSCs under chondrogenic conditions. LIG, AC and GP ECM scaffolds were seeded with 500,000 FPSCs per scaffold. Constructs were cultured in the presence of **chondrogenic media** (containing TGF-β3) for 28 days. AC-ECM scaffolds demonstrated the greatest GAG and type II collagen deposition as demonstrated by both (**A**) histological and immunohistochemical staining and (**B-D**) biochemical quantification. AB = Alcian Blue (sGAG). PR= Picrosirius Red (Collagen). AR = Alazarin Red (Mineral deposition). Scale bar = 200 μm. All data is represented as Mean ± SD for ≥6 scaffolds. Statistical differences were assessed using one-way ANOVA with Tukey post-test. *$p < 0.05$, **$p < 0.01$, ***$p < 0.001$.

percentage of $CCR2^{+}CX3CR1^{+}$ macrophages were observed in defects treated with GP:LIG-ECM scaffolds (Fig. 7 A & B). While CCR2 is typically associated with a more M1-like phenotype, CX3CR1 is expressed by M2 or anti-inflammatory macrophages,[39,40] and therefore co-expression of these markers is suggestive of a distinct hybrid M1-M2 macrophage phenotype. This was also reflected in the level of expression of these surface markers with a significant increase in median fluorescence intensity (MFI) of both CCR2 and CX3CR1 in macrophages from rats that had been implanted with GP:LIG-ECM scaffolds, compared to that of empty and AC-ECM scaffolds (Fig. 7C & D). This suggests that not only is there a higher pool of cells double positive for CCR2 and CX3CR1, but that the activity and the level of expression of these receptors are also enhanced. Surface expression of CD86 and MHCII, remained unchanged across each experimental group (Fig. S 5). In order to provide more

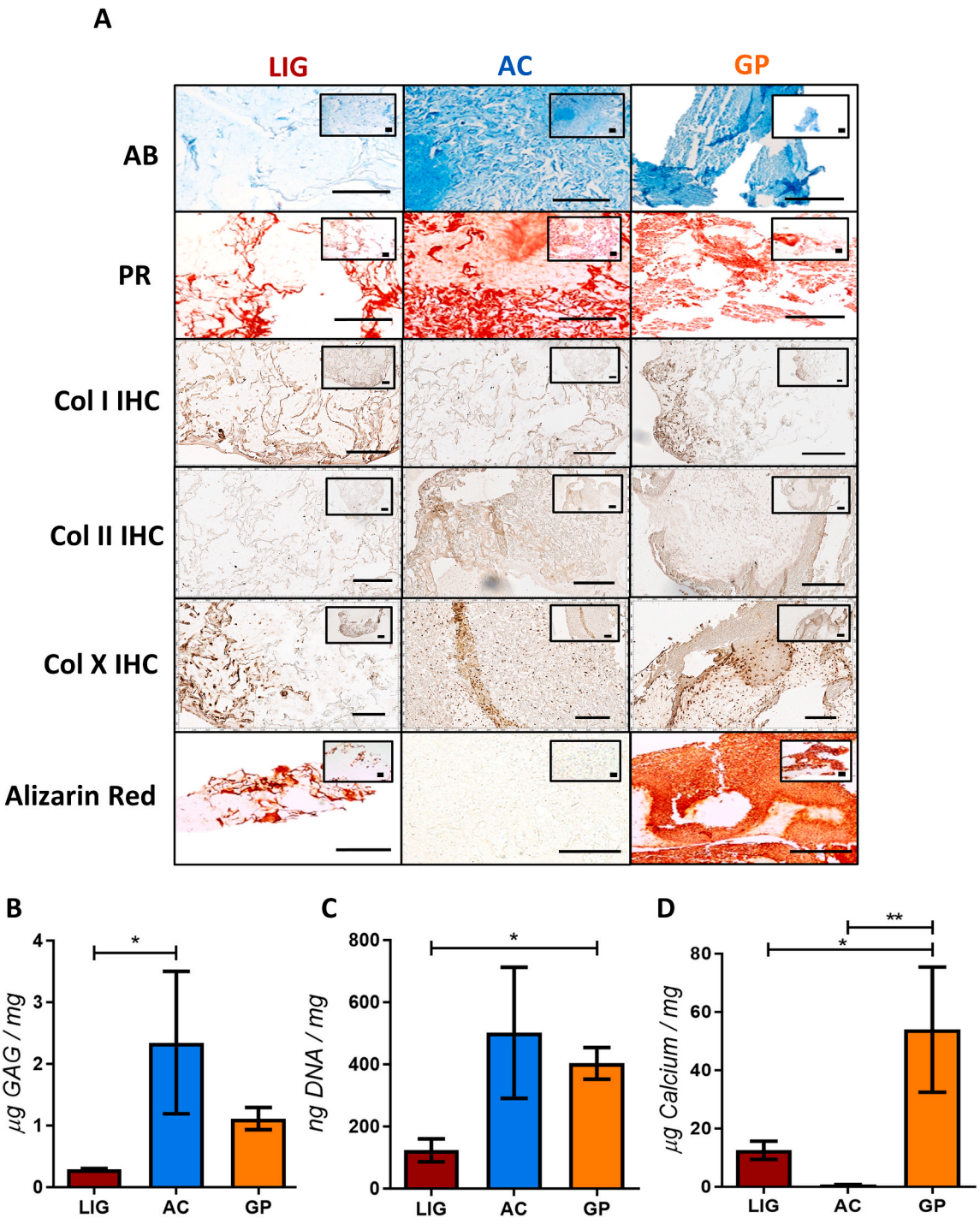

Fig. 5. GP-ECM scaffolds promote robust osteogenic differentiation of BM-MSCS under osteogenic conditions. LIG-, AC- and GP-ECM scaffolds were seeded with 500,000 BM-MSCs per scaffold. Constructs were cultured in the presence of **osteogenic media** (containing β-Glycerophosphate) for 28 days. GP-ECM scaffolds demonstrated the greatest calcium deposition as demonstrated by both (**A**) histological and (**B-D**) biochemical quantification. AB = Alcian Blue (sGAG). PR= Picrosirius Red (Collagen). AR = Alizarin Red (Mineral deposition). Scale bar = 200 μm. All data is represented as Mean ± SD for ≥6 scaffolds. Statistical differences were assessed using one-way ANOVA with Tukey post-test. *$p < 0.05$, **$p < 0.01$, ***$p < 0.001$.

extensive characterisation of the macrophage phenotype, we analyzed CD206 and CD80 expression, as additional M2 and M1 markers respectively, on tissue slices. Using CD68 as a pan macrophage marker, immunofluorescent staining revealed that macrophages present in the empty defect did not express high levels of CD206, with AC-ECM and GP:LIG-ECM implanted rats displaying comparable positive staining. Interestingly, macrophages from rats implanted with GP:LIG-ECM scaffolds were the only group with CD80 marker expression, which was absent from both empty control and AC-ECM implanted groups (Fig. 7 E). Taken together, these data supports our findings from the *in vitro* studies and suggests that AC-ECM scaffolds are supportive of an M2 macrophage phenotype, while GP:LIG-ECM scaffolds are polarizing macrophages towards a distinct hybrid M1-M2 macrophage phenotype *in vivo*.

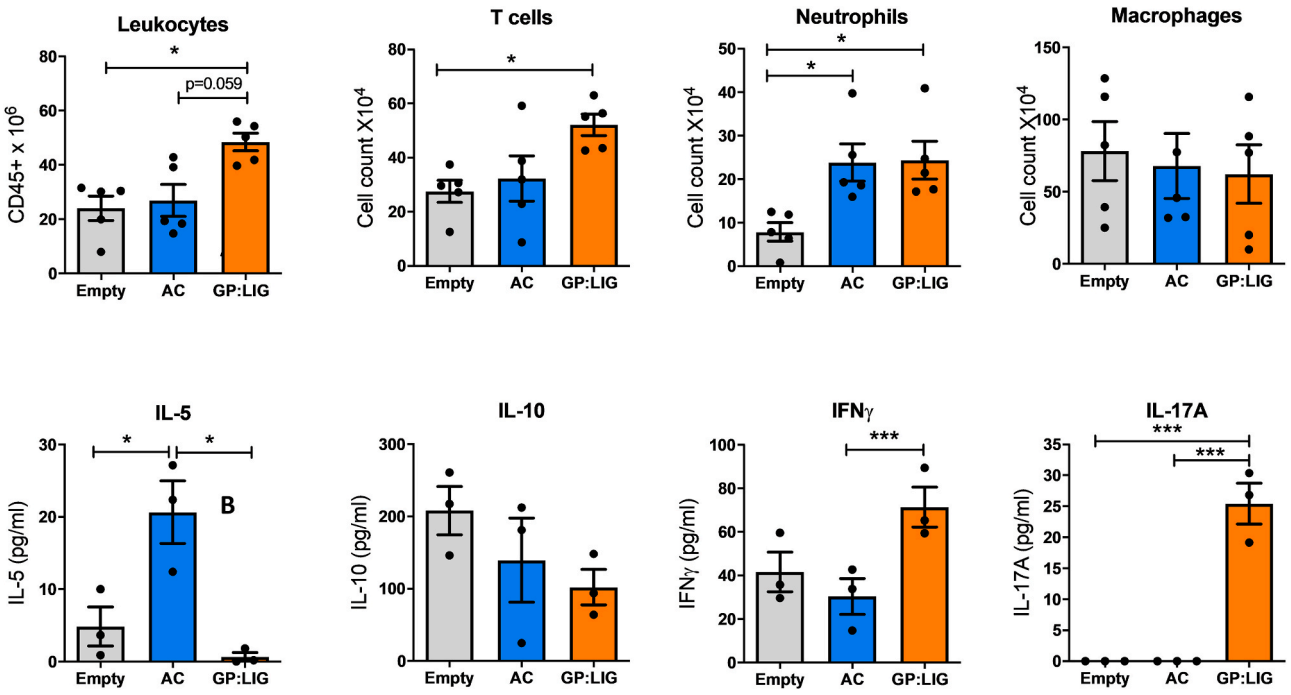

Fig. 6. Characterisation of immune cell subsets and systemic serum cytokine production following implantation of ECM scaffolds into a rat femoral defect model. (A) Implanted ECM scaffolds were harvested from defect site by punch biopsy 1 week post implantation, digested with a collagenase digestion cocktail and isolated cells were stained with immunofluorescent panel of antibodies. Absolute numbers of $CD45^+$ leukocytes, $CD3^+$ T cells, $Ly6G^+$ neutrophils and $CD11b^+F4/80^+$ macrophage populations within the defect site were quantified by flow cytometry 1 week post-implantation. **(B)** Cardiac punctures were performed and serum was isolated from blood samples. IL-5, IL-10, IFNγ and IL-17 cytokine levels were measured by ELISA. All data is represented as Mean ± SEM (n = 3–5 rats) and statistical differences were assessed using Kruskal Wallis test with Dunn's post-test, *$p < 0.05$, ***$p < 0.001$.

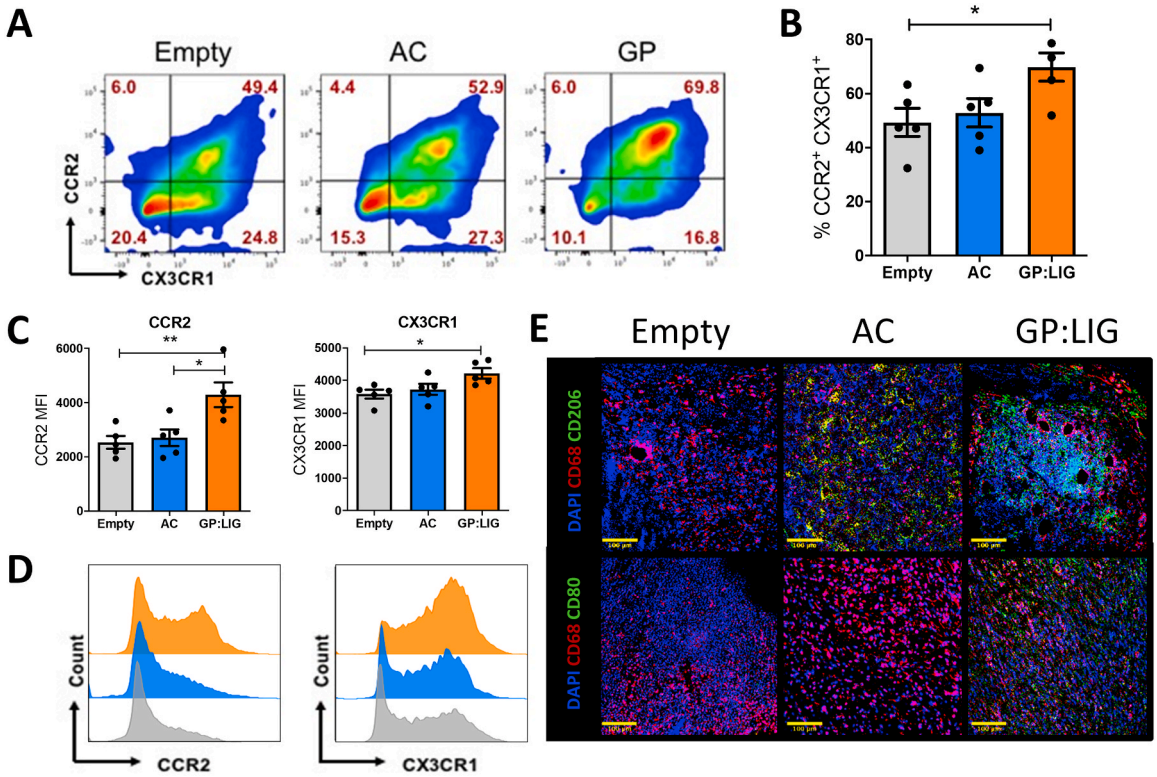

Fig. 7. GP derived ECM scaffolds promote a hybrid M1/M2 phenotype after implantation into a rat femoral defect. (A) Representative dot plots (with mean population percentages, n = 5) depicting CCR2 and CX3CR1 staining of macrophages 1 week post ECM scaffold implantation. **(B)** Quantification of mean (n = 5) $CCR2^+$ $CX3CR1^+$ macrophages. **(C)** Analysis of macrophage population at defect site expressing CCR2, CX3CR1, CD86 and MHCII with **(D)** representative histograms of each marker. **(E)** Immunofluorescent staining for CD68 (pan macrophage marker), CD80 (M1 marker) and CD206 (M2 marker). All data is represented as Mean ± SEM (n = 5 rats). Statistical differences were assessed using Kruskal Wallis test with Dunn's post-test, *$p < 0.05$, **$p < 0.01$.

3.7. GP:LIG-ECM scaffolds promote vascularisation and formation of mature vessels

We have previously demonstrated that higher numbers of CX3CR1 M2-like macrophages at the defect site correlates with enhanced vascularisation.[23] While M2 macrophages are typically associated with tissue regeneration, the specific contributions of different macrophage phenotypes to angiogenesis still remains largely unknown.[33,41,42] We demonstrated that in an *in vitro* system, GP:LIG-ECM scaffolds were capable of promoting growth factors and cytokines associated with vascularisation and angiogenesis, while also driving a hybrid M1-M2 macrophage phenotype. Given the complex role of macrophage phenotype in angiogenesis and vascularisation, we next sought to determine whether the different macrophage phenotypes we observed also coincided with enhanced vascularisation. H&E stained tissue revealed homogenous cell infiltration in all experimental groups 1 week post implantation. Little to no vessels were observed in rats implanted with AC-ECM scaffolds, however the presence of vessels was apparent in the GP:LIG-ECM scaffold group (Fig. 8 A). When quantified, GP:LIG-ECM scaffolds contained significantly more vessels than both AC-ECM scaffolds and empty defect (Fig. 8 B). Furthermore, vessels in the GP:LIG-ECM group appeared mature, as evidenced by von Willibrand Factor (vWF) and α -smooth muscle actin (α-SMA), in comparison to immature vessels, only staining positive for vWF clotting factor in the empty defect (Fig. 8C & D). Analysis of the total number of cells that were double-positive for vWF and α-SMA was significantly higher in GP:LIG-ECM group in comparison to immature singly stained vWF vessels that were present in the empty defect tissue. Taken together this suggests that GP:LIG-ECM scaffolds are supportive of a more mature vessel formation at this early timepoint. No differences in the levels of bone formation, as evident by μCT analysis, were observed at later timepoints (Fig. S 6).

4. Discussion

The overall objective of this study was to elucidate the human MSC and macrophage phenotype upon exposure to ECM biomaterials derived from different musculoskeletal tissue sources. Our findings demonstrate that GP-ECM promotes a hybrid M1-M2 macrophage phenotype, in contrast to AC-ECM exposed macrophages that adopt an M2-like phenotype. Furthermore, ECM scaffolds differentially induced cytokines and growth factor production in primary human macrophages and were capable of directing the differentiation of MSCs towards the phenotype of their source tissue, with AC-ECM promoting chondrogenesis and GP-ECM promoting osteogenic differentiation. *In vivo* phenotyping mirrored that of the *in vitro* studies, with implantation of AC-ECM scaffolds driving an M2-like phenotype in contrast to higher numbers of $CD45^+$ leukocytes and $CD3^+$ T cells and $CCR2^+CX3CR1^+$ macrophages in rats implanted with GP:LIG-ECM scaffolds. This provides further evidence that GP-ECM containing scaffolds direct a unique immune profile with a hybrid M1-M2 phenotype. Moreover, enhanced vascularisation and formation of mature vessels was only observed in rats implanted with GP-ECM containing scaffolds indicating that this material has inherent pro-angiogenic properties.

ECM based scaffolds have previously been reported to promote an M2-like phenotype both *in vitro* and *in vivo*.[43] However, given the intricate biological and biochemical structure of ECM derived from diverse sources, caution must be taken in drawing broad conclusions

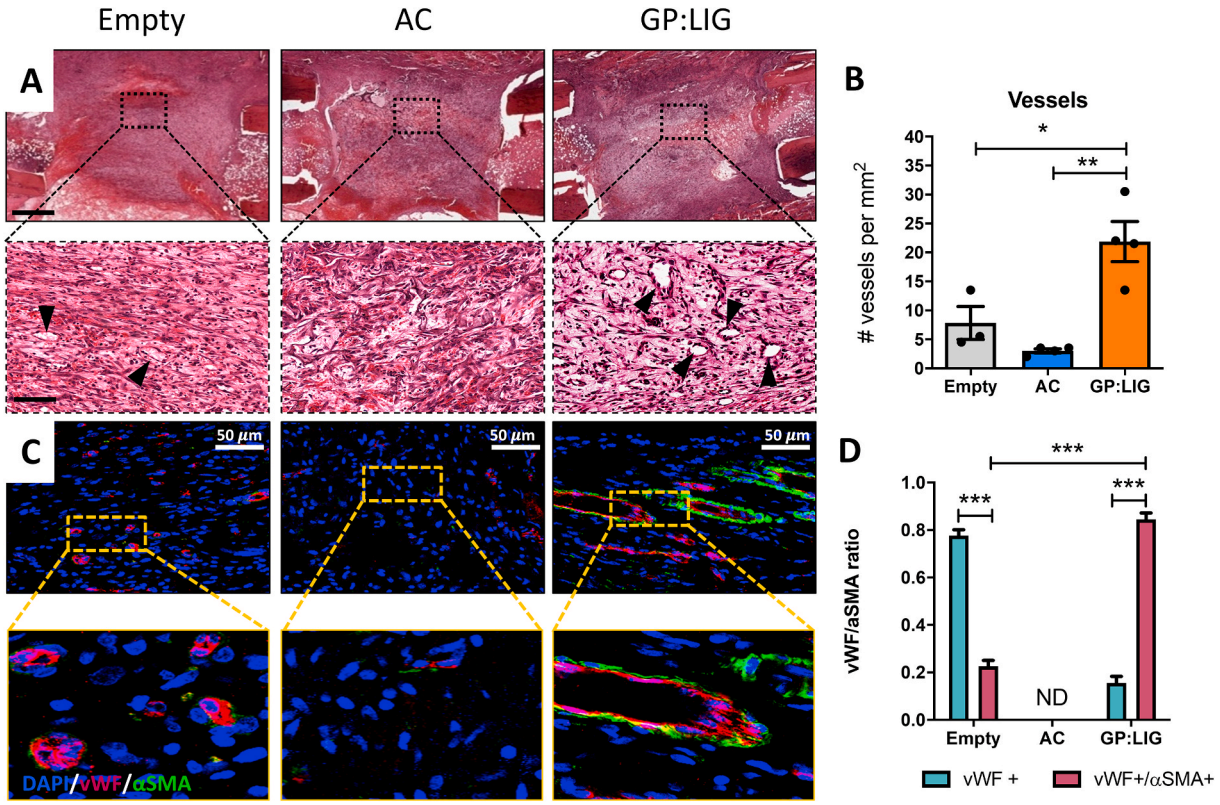

Fig. 8. GP derive ECM scaffolds promote vascularisation following implantation into a rat femoral defect model. (A) Representative images of low magnification H&E stained tissue at the defect site 1-week post-implantation. Images taken at 2x (upper panel, scale-bar 1 mm) and 10x (lower panel, scale-bar 200 μm). Arrows indicate the presence of vessel structures. **(B)** Quantification of total number of vessels from H&E stained tissue slices (data points represent average vessel number, averaged from 2 tissue slices per rat in a ROI of 2 × 2 mm, per rat (n = 4)). **(C)** Representative images of vessel formation 1 week post implantation. von Willibrand Factor (vWF) shown in red, α-smooth muscle actin (α-SMA) in shown in green and DAPI in blue. Scale bar = 50 μm. **(D)** Ratio of single positive (vWF) to double positive (vWF/α-SMA) vessels (determined across 10 fluorescent images per rat (n = 3 rats) as an indication of vessel maturity. All data is represented as Mean ± SEM and statistical differences were assessed using one-way ANOVA with Tukey post-test. *p < 0.05, **p < 0.01, ***p < 0.001.

regarding their M2 immunomodulatory capacities. The inherent immunomodulatory capacity of AC, LIG and GP-ECM was found to induce diverse macrophage phenotypes *in vitro* with LIG-ECM appearing to be the most biologically inert of the three types of ECM with no capacity to modulate macrophage phenotype. AC-ECM resulted in enhanced expression of the M2-associated markers, which was in contrast to GP-ECM exposed macrophages, which appeared to co-express M1 and M2 markers, demonstrating a distinct hybrid polarization state. This phenomenon of distinct macrophage phenotypes by ECM may not be unique to GP-ECM, as Dziki *et al.* have recently demonstrated that solubilised ECM from diverse tissue sources do not exclusively drive an M2 phenotype.[14] ECM derived from skeletal muscle, liver and dermis were found to have a reduced capacity to upregulate M2 markers Fizz 1 and CD206 and also exhibited higher expression of the M1-like marker iNOS. Unlike the findings here, no notable differences in the phagocytic capacities of these ECM treated macrophages was observed,[14] however discrepancies across these two studies may be due to the use of murine bone marrow-derived macrophages in comparison to the blood-derived human macrophages used in the present study.

In addition to inducing distinct macrophage phenotypes, ECMs also induced cytokine production associated with homeostatic processes of their source tissue. Most notably high concentrations of IL-6 and TNF were observed in cell supernatants from GP-ECM exposed macrophages. These two cytokines are normally expressed early after bone injury and can exert pro-osteogenic effects; TNF can promote osteogenic differentiation of human MSCs,[44–46] while IL-6 can act synergistically with BMP2 to promote MSC osteogenesis.[27] In contrast, AC-ECM enhanced the expression of IL-8, which has been shown to have a pro-chondrogenic role[30,31] and bFGF, a well-known chondrogenic factor.

In addition to modifying the secretome of macrophages to create tissue specific regenerative environments, different ECM scaffolds were also found to support distinct MSC phenotypes. Despite the relatively harsh solubilisation and decellularization procedure employed to fabricate the scaffolds and ensure sufficient decellularization, robust chondrogenic differentiation of FPSCs was observed in the AC-ECM scaffolds, while GP-ECM scaffolds supported robust osteogenesis. This indicates that the decellularization procedure applied here, while robust enough to sufficiently decellularize the tissue, does not negatively impact downstream MSC differentiation. Under chondrogenic conditions, no evidence of hypertrophic differentiation (as evidenced by the lack of type X collagen staining) or mineralization was observed across any of the scaffold variants. The AC-ECM scaffold described here has recently been tested in a caprine model of cartilage defect repair, the AC-ECM scaffold successfully improved repair when used in conjunction with the current surgical standard of care for cartilage defects, microfracture, further demonstrating the effectiveness of the AC-ECM scaffold.

In vivo characterisation of immune cell, especially macrophage phenotype, was consistent with *in vitro* findings. Higher concentrations of circulating IL-5 was observed in rats implanted with AC-ECM scaffolds. This cytokine is associated with type-2 immune response, which can suppress type 1-driven inflammation and given the presence of CD206 macrophages, suggests that this ECM scaffold primarily promotes an M2 or type-2 pro-regenerative phenotype *in vivo*. This is consistent with previous studies demonstrating that implantation of an ECM scaffold typically drives M2-like macrophage responses.[1,3,43] Furthermore, it has recently been demonstrated that IL-4, another type 2 cytokine that directs M2 responses, was enhanced upon implantation of ECM scaffolds in a volumetric muscle loss model, which resulted in enhanced tissue healing at the defect site.[47] In contrast, implantation of GP:LIG-ECM scaffolds resulted in higher numbers of $CD45^+$ immune cell infiltration, especially $CD3^+$ T cells. While the exact role of T cells has not been fully elucidated in the context of musculoskeletal tissue regeneration, it has recently been suggested that T cell infiltration is required for effective bone fracture repair, as a certain amount of inflammation is required at an early stage of bone healing.[48–50] Importantly, our *in vitro* cultures demonstrated elevation of the chemokines CXCL9 and CXCL10, which are known to play a role in the recruitment of T cells.[25,26] Interestingly, high concentrations of circulating IL-17 A, potentially from Th17 cells, was observed in rats implanted with GP-ECM scaffolds, a cytokine which has recently been shown to positively influence osteoblast behaviour and bone remodelling.[51–53] GP:LIG-ECM scaffolds were also found to drive a specific hybrid macrophage phenotype co-expressing CCR2 and CX3CR1, which are considered pro-inflammatory M1 and anti-inflammatory M2 markers respectively.[39,40] Consistent with this, It has recently been demonstrated that scaffold associated macrophages express both CD206 (M2-like) and CD86 (M1-like), further supporting that hybrid macrophage phenotypes are induced post-biomaterial implantation.[54]

Defects treated with GP:LIG-ECM scaffolds contained significantly higher numbers of mature vessels compared to both empty control and AC-ECM treated groups. This aligns with the *in vitro* finding that exposure of macrophages to GP-ECM enhances the expression of *VEGF* and *ANG1,* both of which are known to contribute to vascularisation, and blood vessel maturation and stability.[55–58] Previous studies have demonstrated that macrophages are capable of physically interacting with blood vessels and can influence the fusion of sprouting vessels,[59,60] however, there are conflicting reports regarding the contributions of different macrophage phenotypes in angiogenesis. For instance, M2-like macrophages are positively correlated with angiogenesis and can support pericyte differentiation and vessel stabilisation,[61] while M1 macrophages have been shown to enhance vascularisation and angiogenesis, support vessel sprouting[33] while other studies have found them to inhibit angiogenesis.[61,62] Given the tremendous plasticity of macrophages and that they exist on a spectrum of diverse phenotypes, it is not surprising that the contributions of hybrid subtypes will vary immensely. Here we show that the presence of $CCR2^+CX3CR1^+$ macrophages coincided with enhanced vascularisation and mature vessel formation. Consistent with our findings, Graney *et al.* recently demonstrated that macrophages expressing both M1 and M2 markers facilitated anastomosis of engineered blood vessels *in vivo*.[42] While the direct contribution of these macrophages has yet to be established, $CX3CR1^+$ cells have been reported to play a role in neovascularization and the promotion of angiogenesis in a model of hind-limb ischemia,[63] while $CCR2^+$ macrophages can secrete VEGF and induce vascular sprouting in murine models of healing.[62,64] Taken together with the newly attributed role of M1-M2 hybrid macrophage phenotypes in the promotion of vascular networks, these findings suggest that $CX3CR1^+CCR2^+$ macrophages, found GP:LIG-ECM implants, may be directly influencing vessel formation *in vivo*. In spite of this, no significant differences in the levels of bone formation was observed between the control and experimental groups at later timepoints, suggesting that modulating the early immune response and accelerating vascularisation may be insufficient to accelerate bone healing. Future studies will explore whether the immune-modulating characteristics of GP:LIG-ECM scaffolds can be combined with other pro-osteogenic factors to accelerate functional bone regeneration.

5. Conclusions

The findings of this study show that the source tissue of ECM-derived biological scaffolds differentially influences the behaviour of MSCs and macrophages, directing both cellular differentiation and production of growth factors beneficial to the regeneration of their source tissue. Furthermore, we demonstrate the association of enhanced vascularisation with a hybrid M1-M2 phenotype *in vivo*, indicating that diverse macrophage polarization states can drive vascularisation of biological implants. This work underscores the necessity for in-depth characterisation of diverse macrophages phenotypes, not only in the context of vascularisation and angiogenesis, but also for tissue-specific

regeneration. This study provides further insights into the inherent biological properties of ECM-based materials and will help to inform the design and selection of tissue-specific scaffolds for clinical use.

Data availability

The authors declare that all data supporting the finding of this study are available within the paper and its supplementary information.

Declaration of competing interest

The authors declare that they have no known competing financial interests or personal relationships that could have appeared to influence the work reported in this paper.

Acknowledgments

Funding: O.R.M is supported by Trinity College Dublin, Postgraduate Research Scholarship; A. D is supported by the Health Research Board, Ireland (ILP/POR/2017/041); D.J.K is supported by Science Foundation Ireland (12/IA/1554; 12/US/12489; 12/RC/2278_P2), European Research Council ((ANCHOR – 779909, StemRepair –258463 and JointPrinting – 647004)), Enterprise Ireland (CF/2014/4325), K.T.C is supported by the Irish Research Council and K.H.G.M is supported by Science Foundation Ireland (grant 16/IA/4468); This research was co-funded by the European Regional Development Fund (ERDF) under Ireland's European Structural and Investment Funds Programmes 2014–2020.

The authors wish to thank Ciaran Gavagan of the TCD comparative medicine unit for assistance with the rat surgeries and Relinde van Loo for her assistance with macroscopic and SEM imaging. Schematic diagrams were created with Biorender.com.

Appendix A. Supplementary data

Supplementary data to this article can be found online at https://doi.org/10.1016/j.regen.2021.100041.

Author contributions

O.R.M, D.C·B, A. D and D.J.K. conceived the study, designed experiments, interpreted results and wrote the manuscript. O.R.M and D.C·B conducted experiments with laboratory assistance and intellectual input from K.T.C, P.J.D.P, P·P and K·H.G.M. All authors have given approval to the final version of the manuscript.

References

1 Brown BN, Londono R, , et alBadylak F. Macrophage phenotype as a predictor of constructive remodeling following the implantation of biologically derived surgical mesh materials. *Acta Biomater*. 2012;8:978–987.
2 Brown BN, Valentin JE, Stewart-Akers AM, McCabe GP, Badylak SF. Macrophage phenotype and remodeling outcomes in response to biologic scaffolds with and without a cellular component. *Biomaterials*. 2009;30:1482–1491.
3 Sicari BM, Dziki JL, Siu BF, Medberry CJ, Dearth CL, Badylak SF. The promotion of a constructive macrophage phenotype by solubilized extracellular matrix. *Biomaterials*. 2014;35:8605–8612.
4 Julier Z, Park AJ, Briquez PS, Martino MM. Promoting tissue regeneration by modulating the immune system. *Acta Biomater*. 2017;53:13–28.
5 Godwin JW, Pinto AR, Rosenthal NA. Macrophages are required for adult salamander limb regeneration. *Proc. Natl. Acad. Sci. U.S.A.* 2013;110:9415–9420.
6 Schlundt C, El Khassawna T, midt-Bleek, et al. Macrophages in bone fracture healing: their essential role in endochondral ossification. *Bone*. 2015;106:78–89.
7 Sridharan R, Cameron AR, Kelly DJ, Kearney CJ, O'Brien FJ. Biomaterial based modulation of macrophage polarization: a review and suggested design principles. *Mater Today*. 2015;18:313–325.
8 Mahon OR, O'Hanlon S, Dunne CCA, et al. Orthopaedic implant materials drive M1 macrophage polarization in a spleen tyrosine kinase- and mitogen-activated protein kinase-dependent manner. *Acta Biomater*. 2018;65.
9 Spiller KL, Koh TJ. Macrophage-based therapeutic strategies in regenerative medicine. *Adv Drug Deliv Rev*. 2017;122:74–83.
10 Bonnans C, Chou J, Werb Z. Remodelling the extracellular matrix in development and disease. *Nat Rev Mol Cell Biol*. 2014;15:786–801.
11 Badylak SF. Regenerative medicine and developmental biology: the role of the extracellular matrix. *Anat. Rec. B. New Anat.* 2005;287:36–41.
12 Cunniffe GM, Díaz-Payno PJ, Kelly EJ, et al. Tissue-specific extracellular matrix scaffolds for the regeneration of spatially complex musculoskeletal tissues. *Biomaterials*. 2019;188.
13 Keane TJ, Badylak SF. The host response to allogeneic and xenogeneic biological scaffold materials. *J. Tissue Eng. Regen. Med.* 2015;9:504–511.
14 Dziki JL, Wang DS, Pineda C, Sicari BM, Rausch T, Badylak SF. Solubilized extracellular matrix bioscaffolds derived from diverse source tissues differentially influence macrophage phenotype. *J Biomed Mater Res*. 2017;105:138–147.
15 Badylak SF. The extracellular matrix as a biologic scaffold material. *Biomaterials*. 2007;28:3587–3593.
16 Cunniffe GM, Díaz-Payno PJ, Kelly J, et al. Growth plate extracellular matrix-derived scaffolds for large bone defect healing. *Eur Cell Mater*. 2017;33:130–142.
17 Dziki JL, Huleihel L, Scarritt ME, Badylak SF. Extracellular matrix bioscaffolds as immunomodulatory Biomaterials<sup/>. *Tissue Eng*. 2017;23:1152–1159.
18 Benders KEM, van Weeren PR, Badylak SF, Saris DBF, Dhert WJA, Malda J. Extracellular matrix scaffolds for cartilage and bone regeneration. *Trends Biotechnol*. 2013;31:169–176.
19 Browe DC, Mahon OR, Kelly PJJ, et al. Glyoxal cross-linking of solubilized extracellular matrix to produce highly porous, elastic, and chondro-permissive scaffolds for orthopedic tissue engineering. *J Biomed Mater Res*. 2019;107.
20 Deyl Z, Miksík I, Eckhardt A. Preparative procedures and purity assessment of collagen proteins. *J. Chromatogr. B Anal. Technol. Biomed. Life Sci.* 2003;790:245–275.
21 Mahon OR, Kelly DJ, McCarthy GM, Dunne A. Osteoarthritis-associated basic calcium phosphate crystals alter immune cell metabolism and promote M1 macrophage polarization. *Osteoarthritis Cartilage*. 2020;28.
22 Silveira AAA, Mahon OR, Conran CCN, et al. S100A8 acts as an autocrine priming signal for heme-induced human Mφ pro-inflammatory responses in hemolytic inflammation. *J Leukoc Biol*. 2019;106.
23 Mahon OR, Browe DC, Gonzalez T, , et alDunne A. Nano-particle mediated M2 macrophage polarization enhances bone formation and MSC osteogenesis in an IL-10 dependent manner. *Biomaterials*. 2020;239.
24 Badylak SF, Valentin JE, Ravindra AK, McCabe GP, Stewart-Akers AM. Macrophage phenotype as a determinant of biologic scaffold remodeling. *Tissue Eng*. 2008;14:1835–1842.
25 Marshall A, Celentano A, Cirillo N, McCullough M, Porter S. Tissue-specific regulation of CXCL9/10/11 chemokines in keratinocytes: implications for oral inflammatory disease. *PloS One*. 2017;12. e0172821–e0172821.
26 Metzemaekers M, Vanheule V, Janssens R, Struyf S, Proost P. Overview of the mechanisms that may contribute to the non-redundant activities of interferon-inducible CXC chemokine receptor 3 ligands. *Front Immunol*. 2018;8:1970.
27 Huang R-L, Sun Y, , et alLi Q. IL-6 potentiates BMP-2-induced osteogenesis and adipogenesis via two different BMPR1A-mediated pathways. *Cell Death Dis*. 2018;9:144.
28 Kurozumi A, Nakano K, Yamagata K, Okada Y, Nakayamada S, Tanaka Y. IL-6 and sIL-6R induces STAT3-dependent differentiation of human VSMCs into osteoblast-like cells through JMJD2B-mediated histone demethylation of RUNX2. *Bone*. 2019;124:53–61.
29 Glass GE, Chan JK, Freidin A, Feldmann M, Horwood NJ, Nanchahal J. TNF-promotes fracture repair by augmenting the recruitment and differentiation of muscle-derived stromal cells. *Proc Natl Acad Sci Unit States Am*. 2011;108:1585–1590.
30 Yoon DS, Lee K-M, , et alLee JW. Synergistic action of IL-8 and bone marrow concentrate on cartilage regeneration through upregulation of chondrogenic transcription factors. *Tissue Eng*. 2016;22:363–374.
31 Yang A, L Y, , et alXu J. IL-8 enhances therapeutic effects of BMSCs on bone regeneration via CXCR2-mediated PI3k/akt signaling pathway. *Cell Physiol Biochem*. 2018;48:361–370.
32 Shen YH, Shoichet MS, Radisic M. Vascular endothelial growth factor immobilized in collagen scaffold promotes penetration and proliferation of endothelial cells. *Acta Biomater*. 2008;4:477–489.
33 Spiller KL, Anfang RR, Novakovic K, et al. The role of macrophage phenotype in vascularization of tissue engineering scaffolds. *Biomaterials*. 2014;35:4477–4488.
34 Banchereau J, Brier F, , et alPalucka K. Mmunobiology of. *Annu Rev Immunol*. 2000;18:767–811.
35 Schulz D, Severin Y, Zanotelli VRT, Bodenmiller B. In-depth characterization of monocyte-derived macrophages using a mass cytometry-based phagocytosis assay. *Sci Rep*. 2019;9:1925.
36 Murray PJ, Allen JE, Wynn STA, et al. Macrophage activation and polarization: nomenclature and experimental guidelines. *Immunity*. 2014;41:14–20.
37 Olvera D, Sathy BN, Kelly DJ. Spatial presentation of tissue-specific extracellular matrix components along electrospun scaffolds for tissue engineering the bone-ligament interface. *ACS Biomater Sci Eng*. 2020;6:5145–5161.
38 Vinardell T, Sheehy EJ, Buckley CT, Kelly DJ. A comparison of the functionality and in vivo phenotypic stability of cartilaginous tissues engineered from different stem cell sources. *Tissue Eng*. 2012;18:1161–1170.
39 Landsman L, Bar-on L, Agdarsuren A, et al. CX3CR1 is required for monocyte homeostasis and atherogenesis by promoting cell survival. *Blood*. 2009;113:963–972.
40 Geissmann F, Jung S, Littman DR. Blood monocytes consist of two principal subsets with distinct migratory properties frederic. *Immunity*. 2018;129:470–485.

41 Spiller KL, Nassiri S, Novakovic CE, et al. Sequential delivery of immunomodulatory cytokines to facilitate the M1-to-M2 transition of macrophages and enhance vascularization of bone scaffolds. *Biomaterials*. 2015;37:194–207.
42 Graney PL, Ben-Shaul S, , et alSpiller L. Macrophages of diverse phenotypes drive vascularization of engineered tissues. *Sci. Adv.* 2020;6, eaay6391.
43 Huleihel L, Dziki JL, Badylak JGF, et al. Macrophage phenotype in response to ECM bioscaffolds. *Semin Immunol*. 2017;29:2–13.
44 Gerstenfeld LC, Cullinane DM, Barnes GL, Graves DT, Einhorn TA. Fracture healing as a post-natal developmental process: molecular, spatial, and temporal aspects of its regulation. *J Cell Biochem*. 2003;88:873–884.
45 Kon T, Cho TJ, , et alEinhorn A. Expression of osteoprotegerin, receptor activator of NF-kappaB ligand (osteoprotegerin ligand) and related proinflammatory cytokines during fracture healing. *J Bone Miner Res*. 2001;16:1004–1014.
46 Hess K, Ushmorov A, Fiedler J, Brenner RE, Wirth T. TNFalpha promotes osteogenic differentiation of human mesenchymal stem cells by triggering the NF-kappaB signaling pathway. *Bone*. 2009;45:367–376.
47 Sadtler K, Estrellas K, Elisseeff B, et al. Developing a pro-regenerative biomaterial scaffold microenvironment requires T helper 2 cells. *Science*. 2016;352:366–370.
48 Schmidt-Bleek K, Schell H, , et alDuda GN. Inflammatory phase of bone healing initiates the regenerative healing cascade. *Cell Tissue Res*. 2012;347:567–573.
49 Könnecke I, Serra A, El T, , et almidt-Bleek. T and B cells participate in bone repair by infiltrating the fracture callus in a two-wave fashion. *Bone*. 2014;64:155–165.
50 Schlundt C, Reinke S, midt-Bleek S, et al. Individual effector/regulator T cell ratios impact bone regeneration. *Front Immunol*. 2019;10:1954.
51 Croes M, Kruyt MC, Alblas WJ, et al. Interleukin 17 enhances bone morphogenetic protein-2-induced ectopic bone formation. *Sci Rep*. 2018;8:7269.
52 Jo S, Wang SE, , et alKim T-H. IL-17A induces osteoblast differentiation by activating JAK2/STAT3 in ankylosing spondylitis. *Arthritis Res Ther*. 2018;20:115.
53 Kim HJ, Seo SJ, Kim J-Y, Kim Y-G, Lee Y. IL-17 promotes osteoblast differentiation, bone regeneration, and remodeling in mice. *Biochem Biophys Res Commun*. 2020;524:1044–1050.
54 Sadtler K, Allen BW, Estrellas K, Housseau F, Pardoll DM, Elisseeff JH. The scaffold immune microenvironment: biomaterial-mediated immune polarization in traumatic and nontraumatic applications. *Tissue Eng*. 2017;23:1044–1053.
55 Wernike E, Montjove MO, , et alKlenke M. Vegf incorporated into calcium phosphate ceramics promotes vascularisation and bone formation in vivo. *Eur Cell Mater*. 2010;19:30–40.
56 Conway E, Collen D, Carmeliet P. Molecular mechanisms of blood vessel formation. *Trends Biochem Sci*. 2001;22:251–256.
57 Metheny-Barlow LJ, Li LY. The enigmatic role of angiopoietin-1 in tumor angiogenesis. *Cell Res*. 2003;13:309–317.
58 Ponte AL, Marais E, , et alDomenech. The in vitro migration capacity of human bone marrow mesenchymal stem cells: comparison of chemokine and growth factor chemotactic activities. *Stem Cell*. 2007;25:1737–1745.
59 Fantin A, Vieira JM, , et alRuhrberg. Tissue macrophages act as cellular chaperones for vascular anastomosis downstream of VEGF-mediated endothelial tip cell induction. *Blood*. 2010;116:829–840.
60 Hsu C-W, Poché RA, , et alDickinson. Improved angiogenesis in response to localized delivery of macrophage-recruiting molecules. *PloS One*. 2015;10, e0131643.
61 Jetten N, Verbruggen S, Gijbels MJ, Post MJ, De Winther MPJ, Donners MMPC. Anti-inflammatory M2, but not pro-inflammatory M1 macrophages promote angiogenesis in vivo. *Angiogenesis*. 2014;17:109–118.
62 Sindrilaru A, Peters T, R-Kochanek S, et al. An unrestrained proinflammatory M1 macrophage population induced by iron impairs wound healing in humans and mice. *J Clin Invest*. 2011;121:985–997.
63 Park Y, Lee J, Kim J-A, et al. Fractalkine induces angiogenic potential in CX3CR1-expressing monocytes. *J. Leukoc. Biol. jlb.1A0117-002RR*. 2017;103(1):53–66.
64 Willenborg S, Lucas T, , et alEming A. CCR2 recruits an inflammatory macrophage subpopulation critical for angiogenesis in tissue repair. *Blood*. 2012;120:613–625.